ADVANCED FUNCTIONAL MATERIALS
www.afm-journal.de

A Phosphorescent Nanoparticle-Based Probe for Sensing and Imaging of (Intra)Cellular Oxygen in Multiple Detection Modalities

*Alina V. Kondrashina, Ruslan I. Dmitriev, Sergey M. Borisov, Ingo Klimant, Ian O'Brien, Yvonne M. Nolan, Alexander V. Zhdanov, and Dmitri B. Papkovsky**

Monitoring cell and tissue oxygenation is important for the analysis of cell development and differentiation, mitochondrial function, and common (patho)physiological conditions such as ischemia, cancer, neurodegenerative disorders. A number of materials for sensing cellular oxygen (O_2) by optical means have been described in recent years, but the diverse range of biological models and measurement tasks demands more versatile, flexible, and simple O_2 sensors. A new cell-penetrating phosphorescent nanosensor material called MM2 probe is presented. In it, the highly photostable phosphorescent reporter dye Pt(II)-5,10,15,20-tetrakis-(2,3,4,5,6-pentafluorophenyl)-porphyrin (PtTFPP; emission at 650 nm) and poly(9,9-dioctylfluorene) (PFO) fluorophore act as Förster resonance energy transfer (FRET) donor and two-photon antennae are embedded in cationic hydrogel nanoparticles. Such probe formulation provides efficient delivery into the cell and subsequent sensing and high-resolution imaging of cellular O_2 in different detection modalities, including ratiometric intensity and phosphorescence lifetime-based sensing under one-photon and two photon excitation. MM2 probe combines high brightness, photo- and chemical stability, low toxicity, and ease of fabrication and use. Its versatility and analytical performance are demonstrated in physiological experiments with adherent cells and neurospheres representing 2D and 3D respiring objects and detection on time-resolved fluorescent readers, confocal and multiphoton microscopes, and customized microsecond fluorescence/phosphorescence lifetime imaging microscopy (FLIM) systems.

1. Introduction

Cellular oxygen (O_2) is involved in many vital physiological processes, including oxidative phosphorylation, ATP and reactive oxygen species production in the mitochondria, numerous enzymatic transformations, signalling, regulation of ion fluxes.[1–4] Changes in oxygenation may contribute to neurological disorders such as ischemia, stroke, Alzheimer's and Parkinson's diseases, cardiovascular, psychiatric, and inherited eye disorders.[1,5–7] Therefore, measurement of oxygenation and changes in O_2 consumption rate (OCR) in cells and complex biological objects is important. Here optical probes and techniques allow non-invasive and accurate quantification and imaging of cellular O_2.[8–11]

Common detection modalities in O_2 sensing are phosphorescence intensity, ratiometric and lifetime measurements.[9,11,12] The intensity based platforms are widely available, they are rather simple and suitable for qualitative and semi-quantitative O_2 measurements, but hard to standardize and use for accurate readout of O_2 concentration. Ratiometric intensity measurements at two different wavelengths allow for more stable calibration, since O_2 concentration is calculated from the ratio of the O_2 sensitive and reference luminescent signals.[13,14] However, this ratio can also be influenced by the sample and detection system, e.g., detector noise and blank signals different photobleaching rates, scattering and autofluorescence in the two spectral channels. Phosphorescence lifetime-based detection is by far regarded as more reliable and stable modality for O_2 sensing and imaging,[11,15,16] however such systems operating in the microsecond time domain are still rare, unlike the nanosecond FLIM (fluorescence/phosphorescence lifetime imaging microscopy). With respect to the optical setup, wide-field fluorescence microscopy, which allows 2D imaging, has been extended by the laser-scanning confocal and two-photon systems providing 3D and 4D (with time lapse) O_2 imaging capabilities (also in

A. V. Kondrashina, Dr. R. I. Dmitriev,
Dr. A. V. Zhdanov, Prof. D. B. Papkovsky
Biochemistry Department
University College Cork, Cork, Ireland
E-mail: d.papkovsky@ucc.ie
Dr. S. M. Borisov, Prof. I. Klimant
Institute of Analytical Chemistry and Food Chemistry
University of Technology, 8010 Graz, Austria
I. O'Brien, Dr. Y. M. Nolan
Anatomy and Neuroscience Department
University College Cork, Cork, Ireland

DOI: 10.1002/adfm.201201387

FLIM mode), deep penetration in live tissue, and reduced photodamage to the probe and biological objects.[16,17]

These detection platforms require dedicated phosphorescent O_2-sensitive materials. Examples of such materials include small molecule structures,[12,18] shielded dendrimers,[15,19,20] conjugates with macromolecules (e.g., albumin, PEG, polysaccharides[21]) and delivery vectors (short amino acid sequences, longer peptides, receptor moieties[22,23]). Alternatively, sensor chemistry can be incorporated in micro- and nanoparticle structures that deliver the probe to the cell or tissue compartment, act as quenching matrices, and shield the dye molecules from interferences.[24,25] So far, a number of probes based on ruthenium(II) complexes, PtCP, Pt(II)-octaethylporphin (PtOEP), Pd(II)-meso-tetra-(4-carboxyphenyl)tetrabenzoporphyrin (PdTCPTBP) and Pt(II)-5,10,15,20-tetrakis-(2,3,4,5,6-pentafluorophenyl)-porphyrin (PtTFPP) indicator dyes have been described, designed specifically for sensing of extracellular (EC) and intracellular (IC) O_2 pools, but still they cannot satisfy all the requirements and systems for O_2 measurement.[26]

Thus, dendrimeric probes based on PdTCPTBP and PdTCPP (cell penetrating peptide; oxyphors) have been designed for in vivo monitoring of oxygenation of vasculature, brain and other tissues.[15,19,27] In order to improve two-photon absorption, water-solubility and inertness, additional antennae dye and polyethylene glycol (PEG) coat were added to produce a probe called PtP-C343.[16] Demonstrating excellent analytical performance on a custom-built FLIM platform, these probes still possess drawbacks including longwave emission (above 700 nm, which is problematic for some detectors), moderate photostability, very complex synthesis procedure and no penetration inside the cells.[28]

Intracellular (icO_2) probes are useful for monitoring local oxygenation of cells and O_2 gradients.[25,26,29,30,31] Once-off loading eliminates the need to keep the probe in bathing solution during the experiment.[26,30,31] The main requirements for icO_2 probes are high cell-penetrating ability, low working concentrations, low toxicity and invasiveness (particle size <100 nm produces minimal cell damage[32]), defined mechanisms of cellular entry and localization, optimal response to O_2 and convenient spectral characteristics. The existing icO_2 probes satisfy only some of these requirements, they often rely on non-specific transport mechanisms (phagocytosis, endocytosis, diffusion or partitioning) and display high cell specificity.[11]

First ratiometric nanoparticle icO_2 sensors (called PEBBLEs) were produced by biologically localized embedding and sol-gel technology using a luminescent ruthenium complex and delivered into the cell using a "gene-gun" technique.[33] Aiming to improve performance, some other dye combinations, polymer materials, surface modifications were tested in PEBBLEs, but they still possess high complexity, low loading efficiency, high working concentrations, cell specificity.[13,34–37]

The NanO2 probe based on PtTFPP dye embedded in cationic hydrogel nanoparticles[25] shows high brightness and photostability, high cell-penetration ability with fast (6-16 h) and efficient staining of various mammalian cells, good performance in O_2 sensing and FLIM without cyto- and phototoxicity. However, this probe does not allow for ratiometric or multiphoton imaging of O_2.

In this study we present a new phosphorescent probe called MM2, which combines the advantages and overcomes the limitations of existing O_2 probes allows sensing and imaging of icO_2 in multiple detection modalities

2. Results and Discussion

2.1. Design, Photophysical, and Cell-Penetrating Properties of MM1 and MM2 Probes

The multimodal icO_2 probes (MM series), which are derived from the NanO2 parent structure,[25] were designed by integrating three complementary functionalities in one nanoparticle structure: i) O_2-sensitive phosphorescent reporter dye, PtTFPP; ii) O_2-insensitive reference fluorophore acting as one- and two-photon light harvesting antennae and FRET donor for PtTFPP; iii) the nanoparticle-forming cationic polymer RL-100, which serves as delivery vector, encapsulation and quenching matrix for the dyes.[25] The main challenge was to find a suitable fluorophore that combines the desired photophysical properties, that is compatible with the fabrication method (solution precipitation forming core/shell nanoparticle)[38] and does not perturb the stability, is cell-penetrating, and has the O_2-quenching properties of the parent nanoparticle structure. To achieve this, two different probe formulations containing coumarin C545T and poly(9,9-dioctylfluorene) (PFO) dyes were produced, termed MM1 and MM2, respectively.

Spectral characteristics of MM1 probe are shown in **Figure 1**. It is excitable at 450–490 nm and emits fluorescence at 510–540 nm (similar to fluorescein isothiocyanate (FITC) and enhanced green fluorescent protein (EGFP)) and phosphorescence at 630–700 nm. The shape of the excitation spectrum (detection at 650 nm) reflects efficient FRET between C545T and PtTFPP in the nanoparticles, thus making MM1 a promising candidate for the ratiometric intensity (520/650 nm) and lifetime based (650 nm) detection of icO_2. To verify this, we exposed adherent mouse embryonic fibroblast (MEF) cells to MM1 (10 μg mL^{-1}, 16 h) and observed effective intracellular accumulation similar to the NanO2 (Figure S1, Supporting Information). However, microscopic analysis revealed that luminescent signals of the two dyes have rather different, non-matching localization patterns, with more diffused fluorescence of C545T in the cytoplasm. From this we concluded that upon cell loading and internalization of MM1, C545T dye leaks from the nanoparticles. Such operational instability makes MM1 unsuitable for quantitative sensing of icO_2, due to possible drift of its photophysical properties and O_2 calibration. Interestingly, without cells the stock of MM1 remained stable over several months of storage at 4 °C, no changes in the excitation spectrum were observed which would indicate dye leakage from the nanoparticles and degradation of the FRET system.

To overcome the drawbacks of MM1, the MM2 probe was prepared and assessed similarly. The nanosensors with the hydrophobic polymeric fluorophore, PFO (known as excellent two-photon antennae[34,39] and ratiometric partner for PtTFPP), produced characteristic excitation spectrum with maxima at 390–405 nm, fluorescence of PFO at 410-450 nm and phosphorescence of PtTFPP at 650 nm (Figure 1). To achieve maximal

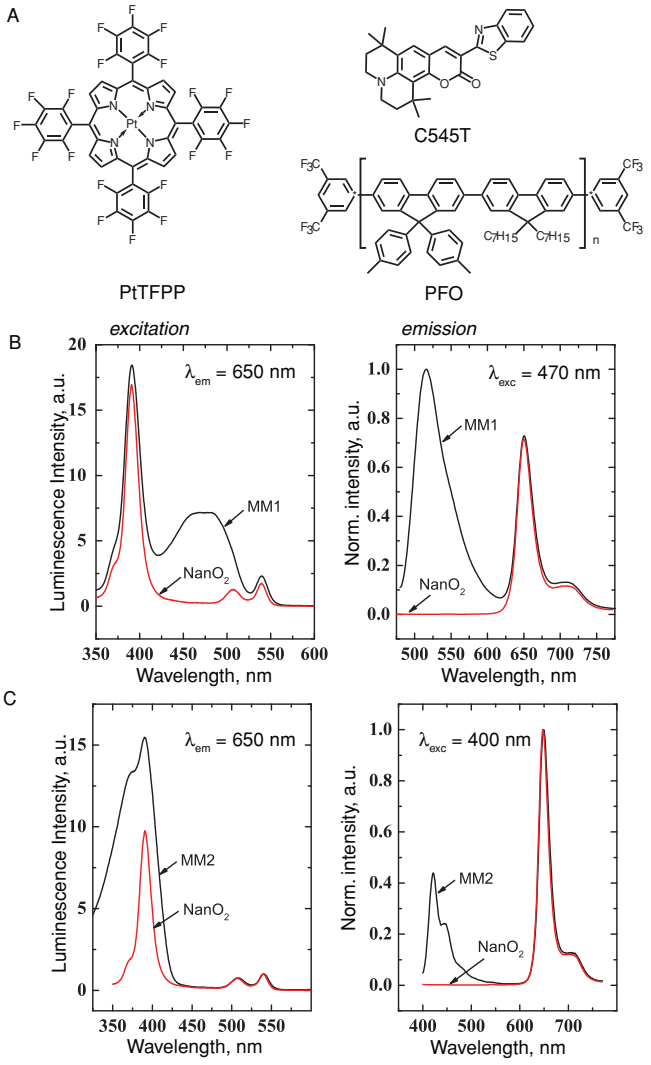

Figure 1. A) Chemical structures of the phosphorescent PtTFPP reporter (1.5% w/w) and fluorescent antennae dyes C545T (1.33% w/w) and PFO (10% w/w). Excitation and emission spectra of resulting B) MM1 and C) MM2 probes.

brightness, FRET efficiency and spectral visibility, concentrations of the two dyes in the nanoparticles were optimized (Figure S2A,B, Supporting Information). PtTFPP content of 1–1.5% w/w produced efficient FRET and strong red phosphorescence when exciting the antenna. For PFO donor 10% w/w concentration provided efficient absorption without aggregation, and strong residual fluorescence that can be used as a reference in ratiometric sensing. Further experiments were performed with this composition of MM2 probe (for comparison, MM1 optimum was 1.33% w/w of C545T and 1% w/w of PtTFPP). When used at the same concentration as NanO2, absorption of MM2 probe was about 2.5 times higher (Figure S2B, Supporting Information), and due to the antennae effect of PFO specific phosphorescence intensity signals from MM2 were similar (Figure 1).

Wide-field and confocal fluorescence microscopy of MEF cells loaded with MM2 revealed stable co-localization of PFO and PtTFPP emissions (**Figure 2**A, B), thus proving that no dye leakage occurs. MM2 stock was stable for at least 6 month of storage at +4 °C, as can be judged from the excitation spectra and phosphorescent signals (data not shown). As determined from the light-scattering experiments (Figure S1C, Supporting Information), MM2 beads had an average size of about 70 nm and homogeneous distribution (PDI = 0.103). This size is somewhat larger than for the NanO2 ($Z_{av} \approx 35$ nm), but well below 100 nm threshold which is regarded safe for the cells.[32] Zeta potential for MM2 particles was +32 mV, which is lower than for the undoped RL-100 beads (+58 mV).

Kinetics of intracellular accumulation of MM2 in MEF cells was found to be similar to that of NanO2, with efficient accumulation in the cytosol after 6-16 h incubation (Figure S3A, Supporting Information). Higher phosphorescent signals (Figure 2A) allowed shorter loading times or lower working concentrations for MM2, which had no influence on cell viability at concentrations up to 30 μg mL^{-1} and exposure times ≤16 h (Figure 2B). Since hypoxia and low O_2 availability may influence probe uptake,[40] we compared loading of MEF cells at 5% and 21% of atmospheric O_2 and found no significant difference (Figure S3B, Supporting Information). Intracellular distribution of MM2 probe in MEF cells was similar to NanO2 probe:[26] perinuclear localization resembling to endoplasmic reticulum and lysosomes and no significant co-localization with the mitochondria (Figure 2C,D). Taken together, MM2 probe accumulates efficiently in mammalian cells, such as MEF cells, and retains its photophysical and O_2 sensing properties.

2.2. Detection of icO_2 with MM2 Probe in Different Modalities

Detection on a time-resolved fluorescence (TR-F) plate reader using rapid lifetime determination (RLD) method[21] and microsecond FLIM microscopy are the most promising platforms for optical O_2 sensing.[11,17,41,42] The first allows simple, high throughput analysis of cell populations, while the second – analysis of individual cells with high spatial resolution and possibility to reconstruct detailed O_2 maps for complex biological samples. Until recently, O_2 FLIM was mainly realized on wide-field microscopes, however laser scanning confocal and multi-photon systems with 3D imaging capabilities are now rapidly emerging.[16,17,41,43] We tested the cells loaded with MM2 probe on these detection platforms and compared the results.

O_2 calibration for MM2 probe loaded in MEF cells generated on Victor2 reader (PerkinElmer) is shown in **Figure 3**A. The range of lifetime changes for MM2 (28–61 μs) was comparable to the NanO2,[26] Stern-Volmer plots also show slightly curved shape. Measured lifetime values were very reproducible (±0.2 μs) and accurate, therefore one time calibration was deemed sufficient. We then monitored local oxygenation of cell layer at 10% of atmospheric pO_2, at rest and upon stimulation with FCCP (carbonyl cyanide 4-(trifluoromethoxy) phenylhydrazone) and AntA (antimycin A) drugs (activator and inhibitor of respiration, respectively). Profiles of phosphorescence lifetime (Figure 3B) and icO_2 concentration (Figure 3C) (calculated using calibration function derived from

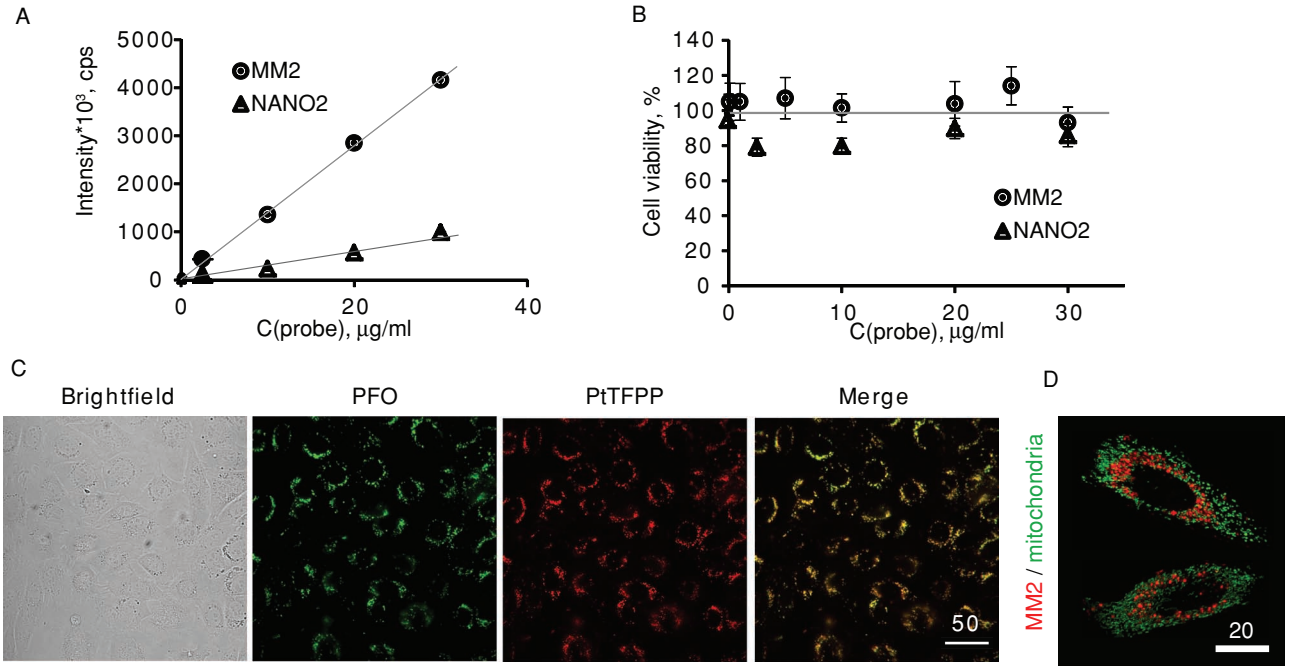

Figure 2. Cell staining properties of MM2 probe with MEF cells. The effect of concentration of MM2 and NanO2 probes (0–30 μg mL^{-1}, 16 h) on A) TR-F signals measured on the microplate reader and B) on cell viability analyzed using a Cell Titer-Glo kit. C) Fluorescent images of MEF cells stained with MM2 (10 μg mL^{-1}, 16 h). D) Analysis of co-localization of MM2 with the mitochondrial marker mitoCase12. Scale bar units are in μm.

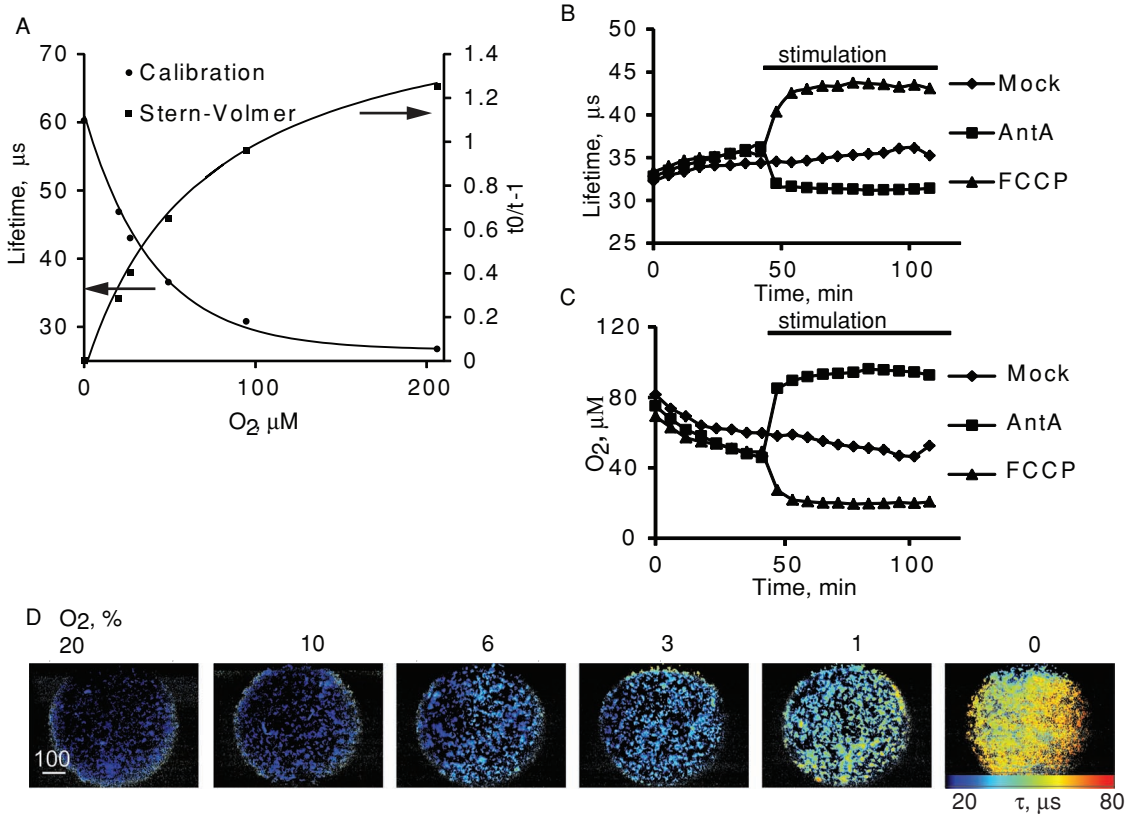

Figure 3. Performance of MM2 probe in phosphorescence lifetime-based of icO_2. A) Phosphorescence lifetime calibration and Stern-Volmer plots generated on Victor2 reader using RLD method. Profiles of B) phosphorescence lifetime and C) icO_2 in adherent MEF cells stained with MM2 probe (2.5 μg mL^{-1}, 16 h), measured at 10% of atmospheric O_2 in microplates. After initial equilibration, cells were stimulated at indicated time points (bars) with 1 μM FCCP, 10 μM AntA or mock (dimethyl sulfoxide (DMSO)) and their respiratory responses were monitored. D) Widefield FLIM microscopy images of MEF cells stained with MM2 (10 μg mL^{-1}, 16 h) measured at different levels of atmospheric O_2 (% indicated). Scale bar unit is in μm.

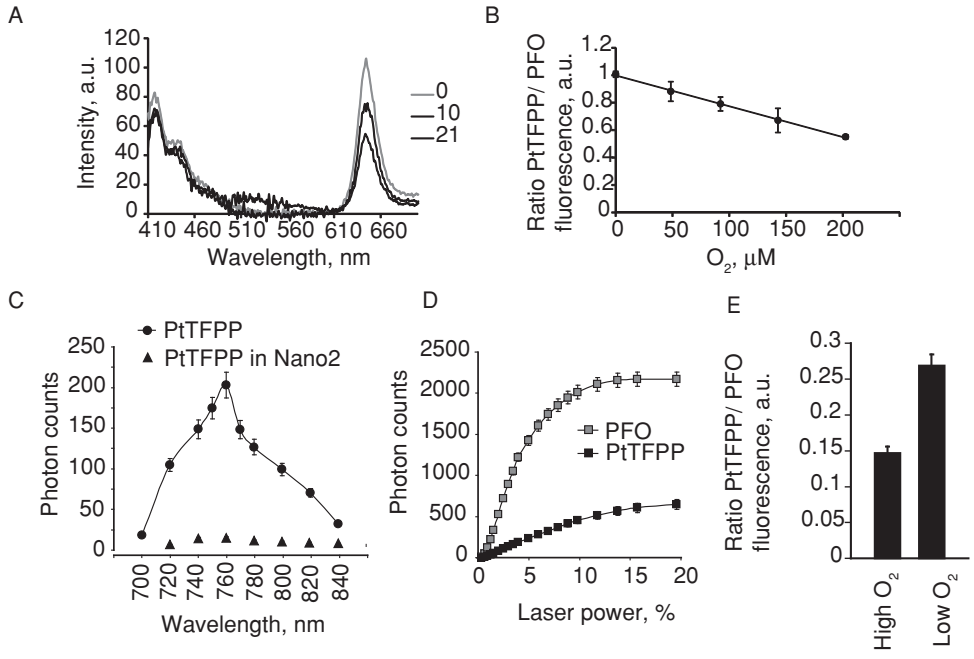

Figure 4. Performance of MM2 probe in ratiometric intensity-based icO2 sensing. A) Emission spectra and B) O_2 calibration for MEF cells stained with MM2 probe (25 μg mL^{-1}, 16 h), measured in suspension on LS-50B spectrometer (PerkinElmer). C) Efficiency of two-photon excitation of PtTFPP dye in MM2 and NanO2 probes at different wavelengths. D) Emission intensitiy of PtTFPP and PFO dyes in MEF cells loaded with MM2 probe measured on multiphoton microscope at different laser power (760 nm). E) Comparison of signal ratio for the cells loaded with MM2 at 21% (high) and 0% (low) O_2.

Figure 3A: $[O_2] = 18\ 861\exp(-\tau/5.79) + 9.62$, Stern-Volmer equation $\tau_0/\tau - 1 = 0.67(1 - 0.04[O_2])$) showed the anticipated effects of reduced O_2 supply and drug treatment, good reproducibility and smoothness.

Next, MEF cells loaded with MM2 probe were measured on a wide-field FLIM system equipped with gated CCD camera and pulsed excitation with 390 nm LED.[43] Figure 3D shows phosphorescent lifetime images of cells at different levels of atmospheric pO_2. Over the range 21–0% O_2, one can see probe lifetime gradually increasing, thus reflecting reduced oxygenation of the cells.

The presence of O_2-insensitive PFO fluorophore in the nanosensors allowed measurement of icO_2 in ratiometric intensity mode. Suspension of MEF cells loaded with MM2 probe measured on a steady-state luminescent spectrometer produced approximately two-fold increase in the emission of the O_2 sensitive dye (650 nm) when changing from air-saturated (21% O_2) to deoxygenated (0% O_2) medium, while PFO fluorescence (410–460 nm) remained steady (**Figure 4**A,B). The changes in intensity ratio were in agreement with lifetime changes (see Figure 3A).

Since Pt-porphyrin dyes have small cross-section of two-photon absorption,[20] by introducing PFO FRET antennae in the phosphorescent nanoparticles we anticipated large improvement in their two-photon excitability with NIR light. Indeed, MEF cells loaded with MM2 and excited with tunable Ti-sapphire laser showed strong PtTFPP emission at around 650 nm and PFO fluorescence at 430 nm, with excitation optimum at around 760 nm (Figure 4C and Figure S4A, Supporting Information). In this mode, MM2 probe was 25-30 times brighter than NanO2 (Figure 4C).

Analysis of PtTFPP and PFO intensity signals in two-photon mode revealed the anticipated quadratic dependence at low laser power (<2%) and saturation at >10% (Figure 4D). In physiological experiments we used 1–1.5% laser power, since over-excitation of the probe can alter the response to O_2 due to over-populated excited states of PtTFPP and damage the cells and probe. Under these conditions resting MEF cells showed increased red fluorescence at 0% O_2 compared to air-saturated conditions, seen as color change from blue to purple (Figure S4B, Supporting Information). Quantitative analysis revealed an approximately two-fold change in the ratio of PtTFPP and PFO signals (Figure 4E). This is consistent with the one-photon excitation data (Figure 4A).

2.3. Physiological Experiments with Neurosphere Culture

The neurosphere culture is a free-floating system comprising of clusters of live neural stem cells in a heterogeneous 3D environment. Neurospheres are a useful experimental tool[44–46] to study the proliferation and lineage fate of neural stem cells, effect of inflammation[47] and ischemia.[48] Localized hypoxia can influence respiration, proliferation, differentiation and signalling of individual cells,[48–50] therefore O_2 imaging in neurospheres is important. We prepared neurospheres from embryonic rat brain with an average diameter of 200–500 μm. These structures showed positive staining with specific markers β-III-tubulin (mature neurons, surface), nestin (neural stem cells, core) or BrdU (proliferating cells) (Figure S5A, Supporting Information). To stain the whole neurosphere rather than cells

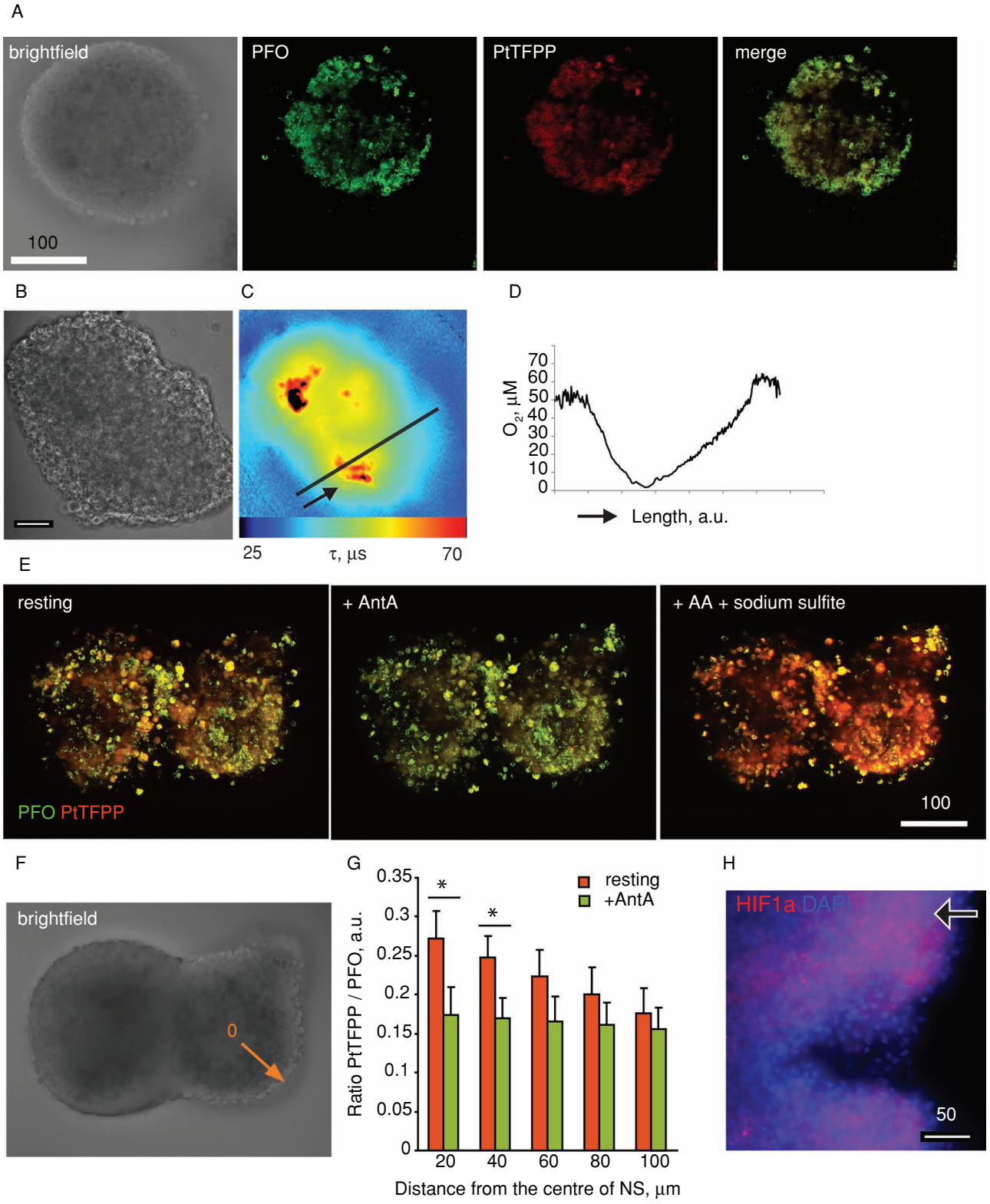

Figure 5. Analysis of oxygenation of neurospheres using MM2 probe. A) Multiphoton microscopy image of one optical slice (5 μm thickness) of a neurosphere stained with MM2 probe. B) Brightfield images, C) lifetime images, and D) profile of O_2 concentration across the neurosphere, measured on the widefield FLIM microscope. E) Ratiometric images of resting and treated (AntA, 5 μM; Na_2SO_3, 5 mg mL^{-1}) neurosphere measured on the multiphoton microscope. F) Brightfield image of the neurosphere and G) PtTFPP/PFO signal ratio at various distances from the core of the neurosphere (indicated with arrow in (F)). H) Image of the neurosphere stained with anti-HIF1α antibody. Neurosphere core is indicated by the arrow. Scale bars are in μm. Asterisks indicate significant differences.

on its surface, MM2 probe was added to the medium during proliferation of neurospheres (**Figure 5**A).

2D mapping of O_2 performed by the wide-field FLIM at 21% of atmospheric O_2 revealed that neurosphere interior (middle part) had largely reduced O_2 levels, i.e., below 30 μM (Figure 5B–D). The area surrounding the neurosphere also had reduced O_2 (≈200 μM), thus indicating that the whole structure respires actively and acts as O_2 sink. The decrease of atmospheric pO_2 in the incubator led to more profound deoxygenation of neurospheres due to limited O_2 supply (not shown). Further analysis by multiphoton microscopy revealed that MM2 localizes inside the neurospheres (Figure 5A,E–G and Figure S5B, Supporting Information), and the signals from the two dyes (PFO, PtTFPP) were co-localized. Again, PtTFPP signals were lower and PtTFPP/PFO ratio was higher at the surface of the neurosphere, thus reflecting its higher oxygenation and limited supply of O_2 to the interior. Inhibition of cell respiration with AntA reduced the signal ratio as a consequence of reoxygenation of the neurosphere, whereas chemical deoxygenation of the medium with sodium sulfite increased the signal ratio (Figure 5E). The presence of hypoxic core of neurosphere was confirmed with positive immunostaining of HIF-1α protein (Figure 5H).

These results demonstrate that oxygenation of the neurosphere, individual cells within it, and cellular responses to metabolic effectors can be measured with MM2 probe in different detection modalities providing useful and biologically relevant information.

3. Conclusions

The multimodal nanoparticle probe MM2, based on the biocompatible polymer RL-100, PtTFPP reporter and PFO antennae dyes, was designed for sensing of icO_2 in respiring samples and evaluated with several common biological models and detection platforms. Compared to the existing probes, MM2 possesses many advantageous features including simple synthesis and use, convenient photophysical properties, high brightness and photostability, efficient cell staining, low toxicity and side effects, general flexibility and optimal sensitivity to O_2. The probe is well compatible with different detection platforms, ranging from simple fluorescent spectrometers and TR-F readers to sophisticated live cell imaging and FLIM systems. It can provide readout of O_2 concentration in luminescence intensity, ratiometric and lifetime based modalities, under one- and two-photon excitation. Lifetime based O_2 sensing and FLIM are regarded as preferred modalities, they provide superior analytical performance and more reliable and accurate quantification of cellular O_2 than. MM2 shows potential for a broad range of physiological experiments and measurement tasks. This nanosensor approach can be explored further to develop probes with other features, for example for low O_2 range, extracellular use or with targeting capabilities.

4. Experimental Section

Materials: PtTFPP and 9,9-diheptylfluorene-2,7-diboronic acid were from Frontier Scientific (USA); coumarin C545T and 3,5-bis(trifluoromethyl) phenylboronic acid were from Aldrich (Austria); 2,7-dibromo-9,9-di-p-tolyl-9H-fluorene from Luminescence Technology (Taiwan); Eudragit RL-100 from Degussa (Germany); tetrakis(triphenylphosphine) palladium (O) = $Pd(PPh_3)_4$ from ABCR (Germany). NanO2 (MitoXpress-Intra) probe was from Luxcel Biosciences (Ireland). Lipofectamine 2000, Opti-MEM I medium, B27 supplement, Alexa Fluor-labelled secondary antibody, ProLong Gold anti-fade medium were from Invitrogen (Bio Sciences, Dun Laoghaire, Ireland). Anti-β-III-tubulin (TU-20, MAB1637), anti-BrdU (BU-1, 05-633) antibodies, fibroblast and epidermal growth factors (FGF and EGF) were from Millipore. MitoCase12 plasmid DNA was from Evrogen (Moscow, Russia). Anti-HIF1a antibody (H1alpha67, NB100-105) was from Novus Biologicals, anti-nestin antibody (R-20, sc-21249) was from Santa Cruz Biotechnology Inc. Standard cell culture grade 96-well plates and white 96 well plates were from Greiner Bio-One (Frickenhausen, Germany). Glass-bottom multiwell inserts were from Ibidi (Martinsried, Germany).

Preparation of the Nanoparticle O_2-Sensitive Probes: MM1 and MM2 probes were prepared similar to the previously described procedure.[25] For the MM1, 2.7 mg of C545T, 2 mg of PtTFPP and 200 mg of Rl-100 were dissolved in 100 mL of acetone and then the particles were precipitated by fast addition of 700 mL water over 2–4 s. For the MM2, 20 mg of PFO (synthesis procedure and main characteristics are described in Supplementary Material), 3 mg of PtTFPP and 200 mg of Rl-100 were dissolved in 45 mL of tetrahydrofurane, then diluted to 100 mL with acetone and precipitated with water. The organic solvents and most of the water were then removed under reduced pressure, to bring probe stock concentration to about 15 mg mL^{-1}.

Cell Culture: Mouse embryonic fibroblasts (MEF) from ATCC (Manassas, VA, USA) were cultured in DMEM media supplemented with 10% FBS, 20 mM 4-(2-hydroxyethyl)-1-piperazineethanesulfonic acid (HEPES) and penicillin-streptomycin. For microscopy collagen-poly-D-lysine coated glass bottom minidishes (MatTek) were used and for the measurements on a TR-F reader - collagen IV-coated 96 well plates. Loading of MEF cells was performed by adding stock of the probe to the medium (typically 10 μg mL^{-1}), incubating the cells for 1–16 h at 37 °C, washing and adding fresh medium. DNA transfection and co-staining with MM2 of adherent MEF cells was performed as described before[26]. Cell viability was assessed by measuring total cellular ATP with a luminescent CellTiter-Glo kit (Promega, WI, USA), according to manufacturer protocol.

Neurosphere Culture: All the procedures with animals were performed under licence issued by the Department of Health and Children (Ireland) and in accordance with the European Communities Council Directive (86/609/EEC). Cortices from embryonic age (E)18 rat embryos (Biological Services Unit, University College Cork) were dissected, and neural stem cells were dissociated, passaged and cultured as neurospheres as previously described.[51] Typically, cortices from 10–14 rat brain embryos were dissected and collected in ice cold Hank's balanced salt solution (HBSS). HBSS was removed and tissue was enzymatically dissociated using 0.1% trypsin–ethylenediaminetetraacetic acid (EDTA) for 15 min at 37 °C. Trypsin inhibitor (0.1% in HBSS) was added, and the solution was tritrated with a flame-polished glass Pasteur pipette, filtered through a cell strainer (BD Falcon, 70 μm nylon filter) and, centrifuged. Cells were resuspended in DMEM/F12 Ham medium supplemented with 2% B27, 20 ng mL^{-1} of EGF and FGF, penicillin-streptomycin and seeded into 25 cm^2 flasks (6–8 × 10^6 cells per flask). The cultures were grown under 21% O_2 for 7 days in vitro (DIV) and half of the medium was replaced every second day. For BrdU staining, 0.2 μM BrdU was added to the culture 18–20 h prior to the analysis. Loading of the neurospheres with the O_2 probes was achieved by adding 20 μg mL^{-1} MM2 to the medium on days 2, 4 and 6. For imaging experiments, neurospheres were collected in a 15 mL tube, washed once, then seeded on poly-D-lysine coated minidishes and allowed to attach. Immunofluorescence staining of the neurospheres was performed by fixing them with 3% paraformaldehyde, permeabilizing with 0.25% Triton X100, staining with specific antibodies, then Alexa Fluor-conjugated secondary antibodies, and 4′,6′-diamidino -2-phenylindole (DAPI), and mounting with ProLong anti-fade reagent.

TR-F Measurements on Microplate Reader: MEF cells were grown in microwells until they reached 80–100% confluence, then loaded with probes and equilibrated in Phenol Red free DMEM (Sigma D5030) medium supplemented with 1 mM L-glutamine, 10 mM D-glucose, 1 mM sodium pyruvate, 20 mM HEPES, pH 7.2, and 10% fetal bovine serum (FBS). The measurements of the probe lifetime, $ic O_2$ monitoring experiments and the calibration inside the hypoxia glove box (Coy Scientific) were performed done as described before[22]. For NanO2 probe, the following calibration function was used $[O_2] = 18\,576\exp(-t/6.8794)$. For ratiometric detection of MM2 probe on Victor2 microplate reader D642 and F460 emission filters and an F355 excitation filter were used.

Fluorescence Microscopy and FLIM Measurements: Probe (co) localization experiments were performed on a laser scanning confocal microscope Olympus FluoView1000 equipped with temperature and CO_2 control. MM2 probe was excited at 405 nm (20–25% laser power) with emission collected at 410–510 nm (PFO) and 600–700 nm (PtTFPP). Fluorescent protein probe MitoCase12 was used to visualize mitochondria, as described previously[26].

Analysis of cell loading kinetics and FLIM measurements were conducted on a wide-field inverted microscope Axiovert 200 (Carl Zeiss, Goettingen, Germany) equipped with gated charge-coupled device (CCD) camera (LaVision BioTec, Germany), excitation module with 390, 480 and 590 nm LEDs (LaVision) and humidified chamber with temperature/CO_2/O_2 control (Pecon). "PtCP" filter cube (excitation 390/40 nm, emission 655/40 nm) was used for imaging PtTFPP phosphorescence, DAPI filter (Semrock 5060B ZHE) for imaging of PFO fluorescence and FITC filter cube (excitation 472/30 nm, emission 535/50 nm) for coumarin C545T fluorescence. FLIM was performed using pulsed excitation with 390 nm LED (10 ms length, 250 ms exposure time and 1×2 binning) with resting and non-respiring (treated with 10 μM AntA) cells at various% of atmospheric O_2. Calibration data points (for AntA-treated samples) were fitted in Origin 6.0 software to determine calibration function. For Stern-Volmer plots (τ_0/τ vs. O_2) the non-linear fitting model was used.[52]

Multiphoton microscopy was performed on the upright multiphoton microscope Olympus FV1000 MPE equipped with a Mai Tai DeepSee Ti:sapphire laser (Newport Corporation, CA), water immersion objective XPLN 25× W NA:1.05 and temperature/CO_2 control. The MM2 and NanO2 probes were imaged in photon count mode (laser power 0.1–20%) using excitation wavelength 690–880 nm with emission collected at 420–460 nm (PFO) and 605–680 nm (PtTFPP). Images were recorded at 20 μs/pixel scanning speed. Cell respiration was inhibited by treatment with AntA, chemical deoxygenation was achieved by addition of KH_2PO_4/Na_2SO_3 (both at 5 mg mL^{-1}) to the medium.

Data Analysis: The data represent average values from at least 6 replicates with standard deviation expressed in error bars. To ensure consistency, all the experiments were performed in triplicate.

Supporting Information

Supporting Information is available from the Wiley Online Library or from the author.

Acknowledgements

This work was supported by the Science Foundation Ireland, grant 07/IN.1/B1804, and EU FP7 Marie Curie ITN Program "Chebana", grant agreement no. 264772.

Received: May 22, 2012
Revised: June 28, 2012
Published online: July 20, 2012

[1] M. D. Brand, D. G. Nicholls, *Biochem. J.* **2011**, *435*, 297.
[2] G. Solaini, A. Baracca, G. Lenaz, G. Sgarbi, *Biochim. Biophys. Acta* **2010**, *1797*, 1171.
[3] A. C. Kulkarni, P. Kuppusamy, N. Parinandi, *Antioxid. Redox Signaling* **2007**, *9*, 1717.
[4] G. L. Semenza, *Biochim. Biophys. Acta* **2011**, *1813*, 1263.
[5] I. L. Ferreira, R. Resende, E. Ferreiro, A. C. Rego, C. F. Pereira, *Curr. Drug Targets* **2010**, *11*, 1193.
[6] A. H. V. Schapira, *Lancet* **2012**, *379*,1825.
[7] J. E. Selfridge, L. E, J. Lu, R. H. Swerdlow, *Neurobiol. Dis.* **2012**. DOI:10.1016/j.nbd.2011.12.057.
[8] R. Springett, H. M. Swartz, *Antioxid. Redox Signaling* **2007**, *9*, 1295.
[9] A. Devor, S. Sakadzic, V. J. Srinivasan, M. A. Yaseen, K. Nizar, P. A. Saisan, P. Tian, A. M. Dale, S. A. Vinogradov, M. A. Franceschini, D. A. Boas, *J. Cereb. Blood Flow Metab.* **2012**, *32*, 1259.
[10] X.-d. Wang, H.-x. Chen, Y. Zhao, X. Chen, X.-r. Wang, *Trends Anal. Chem.* **2010**, *29*, 319.
[11] R. I. Dmitriev, D. B. Papkovsky, *Cell. Mol. Life Sci.* **2012**, *69*, 2025.
[12] J. M. Vanderkooi, G. Maniara, T. J. Green, D. F. Wilson, *J. Biol. Chem.* **1987**, *262*, 5476.
[13] X.-d. Wang, H. H. Gorris, J. A. Stolwijk, R. J. Meier, D. B. M. Groegel, J. Wegener, O. S. Wolfbeis, *Chem. Sci.* **2011**, *2*, 901.
[14] J. Napp, T. Behnke, L. Fischer, C. Würth, M. Wottawa, D. M. Katschinski, F. Alves, U. Resch-Genger, M. Schäferling, *Anal. Chem.* **2011**, *83*, 9039.
[15] I. Dunphy, S. A. Vinogradov, D. F. Wilson, *Anal. Biochem.* **2002**, *310*, 191.
[16] O. S. Finikova, A. Y. Lebedev, A. Aprelev, T. Troxler, F. Gao, C. Garnacho, S. Muro, R. M. Hochstrasser, S. A. Vinogradov, *ChemPhysChem* **2008**, *9*, 1673.
[17] A. S. Golub, R. N. Pittman, *Am. J. Physiol. Heart Circ. Physiol.* **2008**, *294*, H2905.
[18] T. Yoshihara, Y. Yamaguchi, M. Hosaka, T. Takeuchi, S. Tobita, *Angew. Chem. Int. Ed.* **2012**, *51*, 4148.
[19] T. V. Esipova, A. Karagodov, J. Miller, D. F. Wilson, T. M. Busch, S. A. Vinogradov, *Anal. Chem.* **2011**, *83*, 8756.
[20] A. Y. Lebedev, T. Troxler, S. A. Vinogradov, *J. Porphyrins Phthalocyanines* **2008**, *12*, 1261.
[21] T. C. O'Riordan, A. V. Zhdanov, G. V. Ponomarev, D. B. Papkovsky, *Anal. Chem.* **2007**, *79*, 9414.
[22] R. I. Dmitriev, H. Ropiak, G. Ponomarev, D. V. Yashunsky, D. B. Papkovsky, *Bioconjugate Chem.* **2011**, *22*, 2507.
[23] U. Neugebauer, Y. Pellegrin, M. Devocelle, R. J. Forster, W. Signac, N. Moran, T. E. Keyes, *Chem. Commun.* **2008**, 5307.
[24] G. Mistlberger, K. Koren, E. Scheucher, D. Aigner, S. M. Borisov, A. Zankel, P. Pölt, I. Klimant, *Adv. Funct. Mater.* **2010**, *20*, 1842.
[25] A. Fercher, S. M. Borisov, A. V. Zhdanov, I. Klimant, D. B. Papkovsky, *ACS Nano* **2011**, *5*, 5499.
[26] R. I. Dmitriev, A. V. Zhdanov, G. Jasionek, D. B. Papkovsky, *Anal. Chem.* **2012**, *84*, 2930.
[27] D. F. Wilson, O. S. Finikova, A. Y. Lebedev, S. Apreleva, A. Pastuszko, W. M. F. Lee, S. A. Vinogradov, *Measuring Oxygen in Living Tissue: Intravascular, Interstitial, and "Tissue" Oxygen Measurements*, Vol. *701*, Springer US, New York **2011**, pp. 53–59.
[28] L. E. Sinks, E. Roussakis, T. V. Esipova, S. A. Vinogradov, *J. Visualized Exp.* **2010**, e1731.
[29] A. V. Zhdanov, V. I. Ogurtsov, C. T. Taylor, D. B. Papkovsky, *Integr. Biol.* **2010**, *2*, 443.
[30] E. G. Mik, J. Stap, M. Sinaasappel, J. F. Beek, J. A. Aten, T. G. van Leeuwen, C. Ince, *Nat. Methods* **2006**, *3*, 939.
[31] E. Takahashi, M. Sato, *Am. J. Physiol. Cell Physiol.* **2010**, *299*, C1318.
[32] Y.-E. K. Lee, R. Kopelman, *Wiley Interdiscip. Rev.: Nanomed. Nanobiotechnol.* **2009**, *1*, 98.

[33] H. Xu, J. W. Aylott, R. Kopelman, T. J. Miller, M. A. Philbert, *Anal. Chem.* **2001**, *73*, 4124.
[34] C. Wu, B. Bull, K. Christensen, J. McNeill, *Angew. Chem. Int. Ed.* **2009**, *48*, 2741.
[35] M. P. Coogan, J. B. Court, V. L. Gray, A. J. Hayes, S. H. Lloyd, C. O. Millet, S. J. A. Pope, D. Lloyd, *Photochem. Photobiol. Sci.* **2010**, *9*, 103.
[36] Y.-E. Koo Lee, E. E. Ulbrich, G. Kim, H. Hah, C. Strollo, W. Fan, R. Gurjar, S. Koo, R. Kopelman, *Anal. Chem.* **2010**, *82*, 8446.
[37] K. B. Guice, M. E. Caldorera, M. J. McShane, *J. Biomed. Opt.* **2005**, *10*, 064031.
[38] S. M. Borisov, T. Mayr, G. Mistlberger, K. Waich, K. Koren, P. Chojnacki, I. Klimant, *Talanta* **2009**, *79*, 1322.
[39] H. Xiang, L. Zhou, Y. Feng, J. Cheng, D. Wu, X. Zhou, *Inorg. Chem.* **2012**, *51*, 5208.
[40] I. Grigoriev, Ka L. Yu, E. Martinez-Sanchez, A. Serra-Marques, I. Smal, E. Meijering, J. Demmers, J. Peränen, R. J. Pasterkamp, P. van der Sluijs, Casper C. Hoogenraad, A. Akhmanova, *Curr. Biol.* **2011**, *21*, 967.
[41] J. Lecoq, A. Parpaleix, E. Roussakis, M. Ducros, Y. G. Houssen, S. A. Vinogradov, S. Charpak, *Nat. Med.* **2011**, *17*, 893.
[42] S. Sakadzic, E. Roussakis, M. A. Yaseen, E. T. Mandeville, V. J. Srinivasan, K. Arai, S. Ruvinskaya, A. Devor, E. H. Lo, S. A. Vinogradov, D. A. Boas, *Nat. Methods* **2010**, *7*, 755.
[43] A. Fercher, T. C. O'Riordan, A. V. Zhdanov, R. I. Dmitriev, D. B. Papkovsky, *Methods Mol. Biol.* **2010**, *591*, 257.
[44] J. Jensen, M. Parmar, *Mol. Neurobiol.* **2006**, *34*, 153.
[45] G. Santilli, G. Lamorte, L. Carlessi, D. Ferrari, L. Rota Nodari, E. Binda, D. Delia, A. L. Vescovi, L. De Filippis, *PLoS ONE* **2010**, *5*, e8575.
[46] S. Ahmed, *J. Cell. Biochem.* **2009**, *106*, 1.
[47] H. F. Green, E. Treacy, A. K. Keohane, A. M. Sullivan, G. W. O'Keeffe, Y. M. Nolan, *Mol. Cell. Neurosci.* **2012**, *49*, 311.
[48] N. Horie, K. So, T. Moriya, N. Kitagawa, K. Tsutsumi, I. Nagata, K. Shinohara, *Cell. Mol. Neurobiol.* **2008**, *28*, 833.
[49] C. Hegewald, R. Alt, S. Hetz, M. Cross, A. Acikgoez, H. Till, R. Metzger, M. Metzger, *Neurogastroenterol. Motil.* **2011**, *23*, e412.
[50] E. E. Bar, A. Lin, V. Mahairaki, W. Matsui, C. G. Eberhart, *Am. J. Pathol.* **2010**, *177*, 1491.
[51] A. Keohane, S. Ryan, E. Maloney, A. M. Sullivan, Y. M. Nolan, *Mol. Cell. Neurosci.* **2010**, *43*, 127.
[52] E. R. Carraway, J. N. Demas, B. A. DeGraff, J. R. Bacon, *Anal. Chem.* **1991**, *63*, 337.